Parametric study of phenomena influencing secondary hydriding during loca transients

Apou Martial Kpemou, Jean Desquines, Tatiana Taurines, Severine Guilbert, M C Baietto, B. Normand, J. Soulacroix, A. Ambard, F. Bourlier

PARAMETRIC STUDY OF PHENOMENA INFLUENCING SECONDARY HYDRIDING DURING LOCA TRANSIENTS

A. M. KPEMOU[1], J. DESQUINES[1], T. TAURINES[1], S. GUILBERT[1], M.C. BAIETTO[2], B. NORMAND[2], J. SOULACROIX[3], A. AMBARD[4], F. BOURLIER[5]
[1]IRSN, Cadarache, St Paul-Lez-Durance, France
[2]INSA Lyon, Université de Lyon, France
[3]EDF, DIPNN – DIRECTION TECHNIQUE, 69363 Lyon CEDEX 07, France
[4]EDF R&D, MMC Department, avenue des Renardières, Moret-Sur-Loing 77818, France
[5]Framatome (Fuel Business Unit), 69007 Lyon, France
Apou-martial.kpemou@irsn.fr

Abstract. Secondary hydriding may occur during Loss of Coolant Accidents (LOCA) when nuclear fuel cladding is exposed to steam at high temperature. Indeed, during a LOCA, the cladding may burst, and the steam ingress results in cladding inner surface oxidation. The hydrogen released during this oxidation can be partly absorbed by the cladding, leading to a localized high hydrogen content. This study aims at characterizing the influence of different parameters on the maximum hydrogen content, localization, and distribution regarding secondary hydriding. The oxidation duration has been studied using an axisymmetric testing procedure reproducing LOCA conditions. Metallographic analysis and hydrogen measurements have been performed. EPMA and µ-LIBS micro-analysis have been used to map oxygen and the hydrogen local content.

Keywords: Secondary hydriding, LOCA, High temperature oxidation, Microanalysis.

1 INTRODUCTION

LOCA, which stands for Loss of Coolant Accident, is a hypothetical accident scenario resulting from a break in the main coolant line between the coolant pump and the reactor pressure vessel. This scenario is considered for the design of the Emergency Core Cooling System (ECCS). During a LOCA transient, the cladding tubes made of zirconium alloy may burst, and the steam ingress leads to the oxidation of cladding inner surface in the vicinity of the burst balloon. The primary work on the subject by Chung & Kassner [1] and Uetsuka [2] has evidenced a phenomenon called secondary hydriding. Indeed, during the oxidation stage of a LOCA, the inner gaseous environment of the cladding is progressively enriched with hydrogen released by the oxidation reaction. At a certain distance from the burst opening, the internal gaseous environment is highly enriched in hydrogen which can be partly absorbed by the cladding leading to a

localized high hydrogen content of a few hundred up to several thousand wppm at the peak[1,2].

Over the last twenty years, several semi-integral LOCA tests have been performed by many nuclear research institutions such as JAEA [2–5], ANL [6], NRC [7], KIT [8,9], EDF R&D [10], and CEA [11]. These semi-integral tests aim to experimentally reproduce LOCA transients, on rods with inserted pellets, and then study the behavior of fuel claddings. These tests have been performed on fuel claddings, including unirradiated and irradiated claddings, using irradiated fuel pellets or mock-up pellets. The complex nature of these tests combined to the uneven deformed cladding geometry obtained after the burst, impedes the direct study of the various parameters influencing secondary hydriding.

In the present work, a dedicated experimental approach has been used to investigate the influence of oxidation duration on secondary hydriding. An axisymmetric testing procedure was developed, reproducing LOCA conditions, including cladding oxidation and the final quench of the sample. Each sample was characterized by a set of post-test analysis. Post-quench material microstructure, including inner and outer oxide layer thickness axial profiles, was characterized using metallography. Hydrogen axial profiles were obtained mainly by Hot Vacuum Extraction (HVE). A sample was analyzed using Electron Probe Micro-Analysis (EPMA) and Micro Laser Induced Breakdown Spectroscopy (μ-LIBS) to map simultaneously oxygen and hydrogen local content in an extended region. The analytical test results can be used to support secondary hydriding modeling using simple and well-defined boundary conditions.

2 MATERIALS AND METHODS

2.1 Materials

The specimens used in this study were cut from a $M5_{\mathbf{Framatome}}$[1] recrystallized cladding with nominal chemical composition described in Table 1. The outer diameter of the cladding tube is 9.5mm and the thickness 0.57 mm.

Table 1. Chemical composition of the studied $M5_{\mathbf{Framatome}}$ cladding.

Nb (wt%)	O (wt%)	S (ppm)	Fe (wt%)
1	0.14	20	0.035

2.2 Sample geometry and constitutive materials

The samples are cut from as-received $M5_{\mathbf{Framatome}}$ cladding tubes and filled with ceramic pellets. The use of undeformed cladding allows separate effect tests to perform parametric studies with a uniform gap between the pellets and the inner cladding

[1] M5 and $M5_{Framatome}$ are trademarks or registered trademarks of Framatome or its affiliates, in the USA or other countries

surface. The mock-up pellets diameter was varied to study the fuel cladding-gap impact on secondary hydriding. Eight mm in diameter porcelain pellets (in average) have been inserted, resulting in a gap of 160 µm. The sample is left open on its upper end, and tightly closed on the lower end with Swagelok cap (see Fig. 1a). The oxidation temperature profile is monitored by a B-type wire thermocouple (TC) welded on the outer surface of the cladding at approximately 10 mm from the opening.

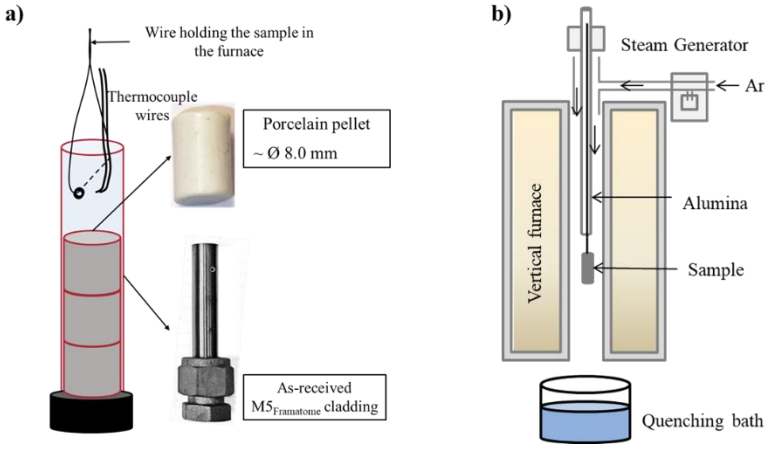

Fig. 1. a) Sample geometry and constitutive materials and **b)** the experimental device and protocol

2.3 High temperature (HT) oxidation

To study secondary hydriding, oxidation tests were performed in steam plus argon environment at approximatively 1200 °C. Each sample is inserted upwards into a vertical furnace under pure argon. After a first fast heating phase, steam is then added to the downstream gas flow to achieve a 50-50% mixture when reaching the target temperature leading to inner and outer cladding surfaces oxidation. The sample is hold for a certain time before quenching (see Fig. 1b). The steam flow rate normalized to the cross-sectional area of the furnace alumina tube was 19.6 $mg.cm^{-2}.s^{-1}$ which is several times above the necessary flow to avoid steam starvation at the outer surface [12].

During the steam oxidation, an oxide layer of zirconia (ZrO_2) is formed on the outer surface of the cladding. On the inner side, the steam ingress, within the narrow pellet-cladding gap, oxidizes the inner surface. Due to the limited space left and gas flow occlusion by argon and hydrogen in the gap, steam starvation occurs in this region. The steam partial pressure progressively disappears replaced by hydrogen partial pressure increase while moving away from the opening. A high hydrogen uptake can then occur at a few millimeters away from the opening, where the inner oxide layer is very thin or absent also corresponding to a high hydrogen partial pressure and probably negligible remaining steam content.

This hydrogen uptake combined with the diffusion process in the material lead to a hydrogen axial profile in the cladding which is called secondary hydriding.

2.4 Post-test characterization

Hydrogen content measurements

After LOCA quenching, nanoscale δ hydride precipitates are located in the samples requiring high resolution microscopy to be observed [1,13]. Consequently, destructive measurement of hydrogen content was used in the present study.

Hydrogen content measurements were then performed by HVE with a LECO ONH 836 analyzer after each oxidation test. The HVE method is based on the extraction of hydrogen gas from a metallic sample by fusion. In this study, the HVE double pic method developed by PSI[2] allows measuring hydrogen content in oxide layers and in the base metal of the sample was used [14]. Hydrogen axial profiles were obtained by measuring hydrogen content in well-localized small cladding pieces cut at different axial positions (see Fig. 2). Calibration of the analyzer is always made before a set of measurements by means of hydrogen-certified standard samples. The average hydrogen content uncertainty is 8% which is the uncertainty of the hydrogen standard content.

Metallographic analysis

Optical metallography is used to measure both inner and outer oxide layer thicknesses after high temperature oxidation. It also allows the identification of the different phases of the material due to oxidation and quenching (oxide layer, α(O)-phase and prior β-phase). These measurements were performed using a Keyence VHX 5000 optical microscope (see Fig. 2).

EPMA & µ-LIBS micro-analysis

The local oxygen content in the different phases of the material was measured by Electron Probe Micro-Analysis (EPMA) with a CAMECA SX-100 Castaing microprobe. This analysis was performed on one sample. Additionally, the local content of iron and niobium was also measured. A surface area of 6000 µm x 600 µm was mapped with a resolution of 2 µm.

Micro-Laser Induced Breakdown Spectroscopy (µ-LIBS) analysis was also carried out by LASALYS. Oxygen and hydrogen maps were obtained on the sample used for EPMA analysis in order to have a complete characterization of this sample. The µ-LIBS analysis is based on the interaction of a pulsed laser beam onto the surface sample [15]. A surface of 3000 µm x 600 µm was scanned with a 3 µm lateral displacement step.

[2] Paul Scherrer Institute (PSI)

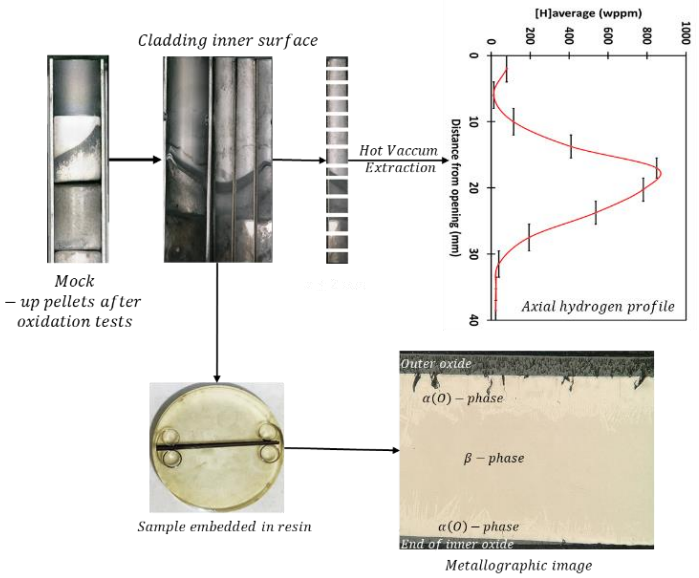

Fig. 2. Analysis methods applied on each sample after oxidation tests

2.5 Test matrix

Eight oxidation tests were conducted for different oxidation duration. These tests allowed studying the influence of oxidation duration on secondary hydriding. The oxidation temperature was set at 1200°C. The temperature measured by the welded TC ranged from 1160°C to 1210°C. The tests parameters are summarized in Table 2.

Table 2. Secondary hydriding analytical tests matrix

Sample ID	Average oxidation temperature at TC position (°C)	Oxidation duration (s)	ECR – CP (%)[3] [16]
M5-100	1160	106	8
M5-200	1190	191	13
M5-400-1	1193	387	19
M5-400-2	1197	378	19
M5-600	1189	646	24
M5-1000	1210	979	33
M5-1400	1189	1430	36

[3] ECR values are calculated with Cathcart-Pawel correlation in doubled-sided oxidation configuration.

3 EXPERIMENTAL RESULTS AND DISCUSSION

3.1 Metallographic analysis

To determine the distribution of different material phases in the cladding, each oxidized sample underwent metallographic analysis. During the oxidation process, the inner and outer surfaces of the cladding were both oxidized, resulting in the formation of a zirconia layer on the surface, as well as α(O)-phase and β-phase in the metal. However, due to steam consumption along the gap by inner surface cladding oxidation, and also due the steam starvation occurring in the gap (limited space left and gas flow occlusion by argon and hydrogen in the gap), the inner zirconia layer growth process is progressively interrupted after only a few tens of millimeters away from the opening (see Fig. 3).

Fig. 4 shows the evolution of the outer zirconia layer with oxidation duration at the thermocouple position. At high temperature, as expected according to [17], the oxide growth rate follows a parabolic law.

3.2 Influence of oxidation duration on secondary hydriding

The main results related to hydrogen content following oxidation tests are summarized in Table 3. Hydrogen axial profiles were obtained for each sample by means of HVE. For some samples, two profiles were obtained using two parts of the sample at different azimuthal positions as shown in Fig. 2. All the hydrogen axial profiles obtained are summarized in Fig. 5 .

With respect to oxidation duration, the peak hydrogen content increases with a parabolic like kinetics, indicating a fast uptake rate in the first few minutes, followed by a slower uptake rate over time. The total amount of hydrogen uptake by the sample follows the same trend (see Fig. 5b). Since the main source of hydrogen comes from the oxidation of the internal surface of the cladding, and this oxidation follows a parabolic law, one can conclude that the hydrogen supply decreases with time. Also, the internal oxide layer growth may reduce and close the gap and then impede the ingress of steam and the transport of hydrogen in the gap interrupting this way the hydrogen uptake process. This phenomenon related to oxide formation may also explain the decrease of the hydrogen uptake for longer oxidation duration. Hydrogen peak position also appears to shift away from the opening with oxidation duration.

These analytical tests also showed that hydrogen uptake occurs in regions without protective oxide layer, since the hydrogen peak is located after the maximum progress of the internal oxide in the gap (see Table 3).

After long durations, the diffusion process in the material takes over on the hydrogen uptake process. This leads to a broadening of the axial hydrogen profile over time and then reduces the maximum hydrogen content at the peak while the total hydrogen uptake is higher (see Fig. 5b).

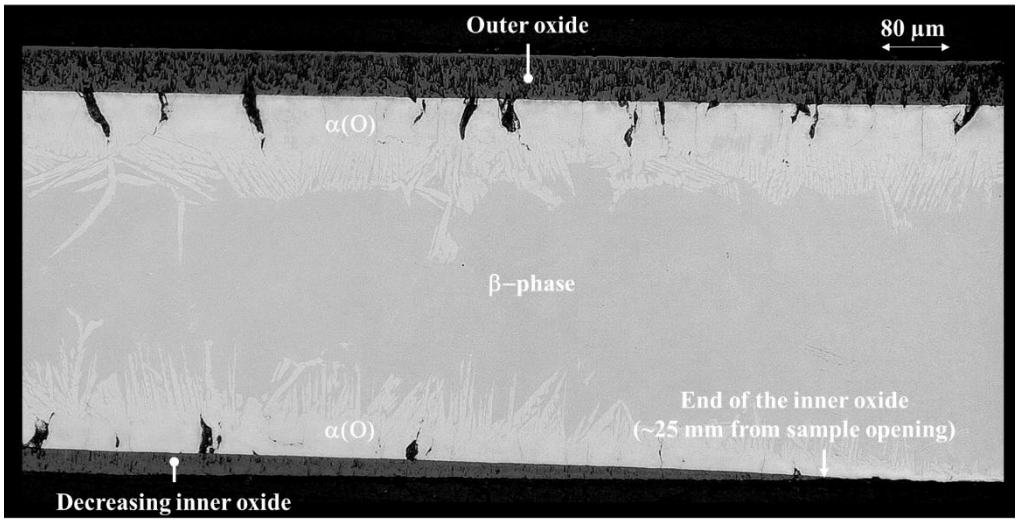

Fig. 3. Metallographic image showing the decreasing and the end of the inner oxide from a sample that underwent oxidation test in LOCA conditions.

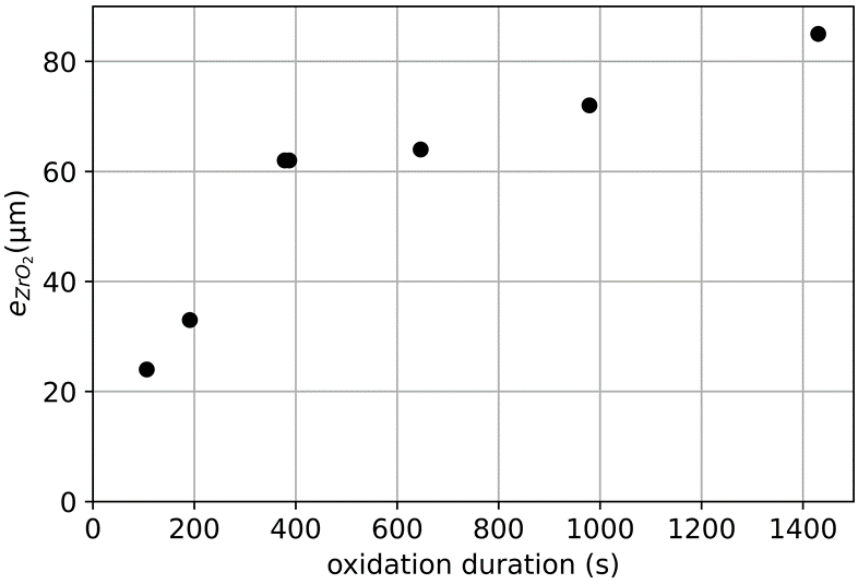

Fig. 4. Outer oxide layer thickness evolution over oxidation duration

Table 3. secondary hydriding results after steam oxidation tests

Sample ID	Peak hydrogen content [H] (wppm)	Integrated hydrogen picked-up (wppm*mm)	Hydrogen peak position from opening (mm ±2)	Inner oxide layer end position from opening (mm)
M5-100	212 ± 19	2316	21	19
M5-200	641 ± 57	6225	16.5	17
M5-400-1	952 ± 82	11066	21	21
M5-400-2	891 ± 73	10869	20	21
M5-600	911 ± 79	14001	22	21
M5-1000	1098 ± 95	15305	25	25
M5-1400	1024 ± 88	18299	22	23

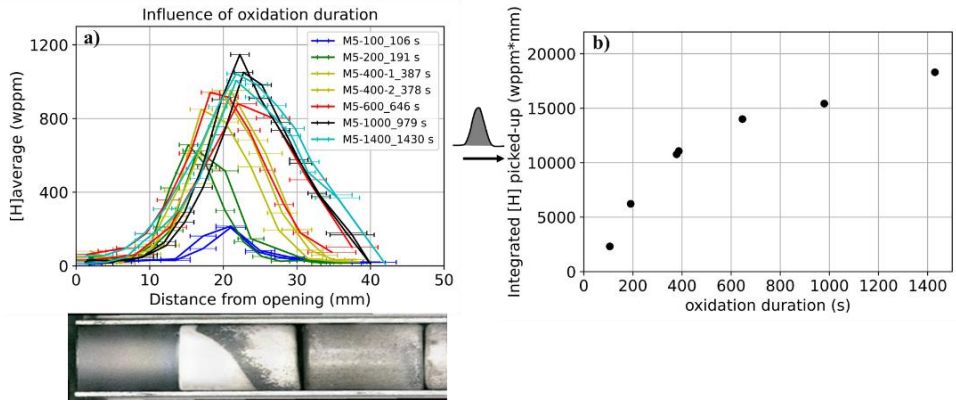

Fig. 5. a) Axial hydrogen profiles and **b)** total hydrogen content uptake by the cladding at different oxidation duration.

3.3 EPMA & µ-LIBS micro-analysis

Oxygen and hydrogen maps were obtained using EPMA and µ-LIBS microanalysis on a sample (Sample ID: M5-400-1) that underwent approximately 400 seconds exposure to steam at 1200°C (see Fig. 6). The analysis was performed at the vicinity of the end the inner oxide layer.

The EPMA analysis was used to measure the local oxygen content in the sample, and this data was used to calibrate the oxygen map obtained from the µ-LIBS analysis. The measured oxygen content in the different material phases is illustrated in Fig. 6a and b. The oxygen maps evidence the decrease up to vanishing of the inner oxide layer and a comparable trend is observed for the internal α(O)-phase layer.

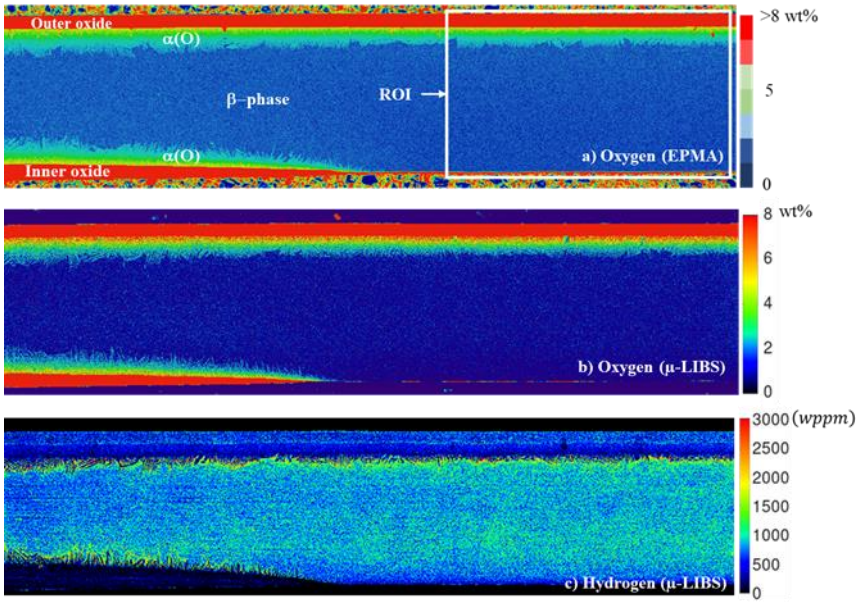

Fig. 6. **a)**- Oxygen maps from EPMA and **b)**- μ-LIBS analysis, and **c)**-hydrogen map from μ-LIBS after ~400s steam oxidation.

Fig. 7 shows the oxygen and hydrogen radial mean contents in the Region Of Interest (ROI, see Fig. 6a) across the cladding thickness. Oxygen content regions above 25 wt.%, mainly covering surfaces exposed to steam, correspond to the oxide layer, the oxygen diffusion from oxide layers stabilizes α(O)-phase at contents below 8% and above 2-3 wt.% and lower contents are associated to the prior β-phase far away from oxygen sources. Higher hydrogen content is observed in the prior β-phase and at the boundary between this phase and the α(O)-phase on the associated profile in Fig.7. This last concentration increases result from low hydrogen solubility of the α(O) layer. The measured hydrogen content in the oxide layer is probably an artefact, since the measurement method wasn't calibrated in oxide layer and the laboratory experience is that very low hydrogen content is expected in this layer (see Fig. 7).

The hydrogen maps when averaged provide consistent measurements with the hydrogen axial profile from HVE (see Fig. 8)

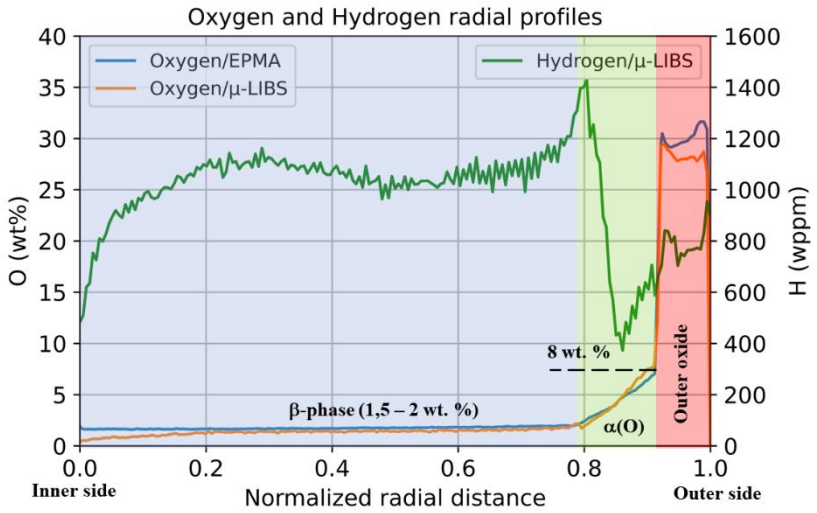

Fig. 7. Oxygen and hydrogen radial distribution in the different phases of the material (in the ROI).

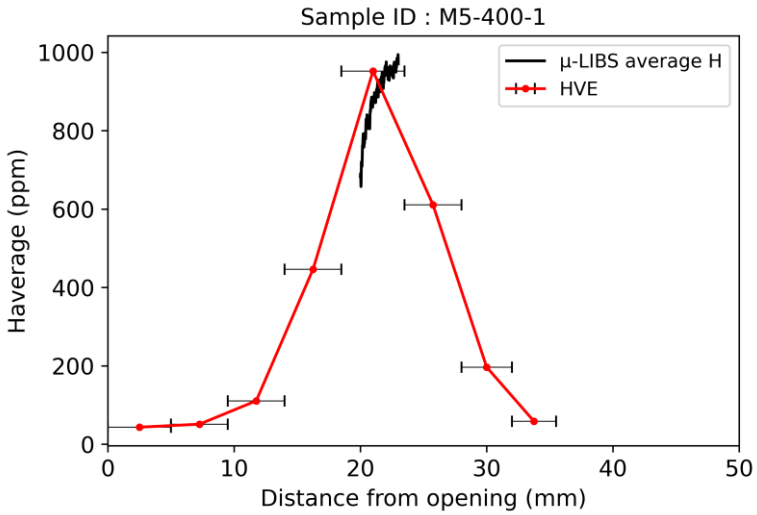

Fig. 8. Comparison between μ-LIBS average hydrogen content and HVE axial hydrogen profile.

4 CONCLUSION

The purpose of this work was to present an experimental approach for studying the parameters influencing secondary hydriding during a LOCA. The influence of oxidation duration was the focus of the paper. It was investigated through oxidation tests performed under conditions comparable to the ones expected during LOCA. The results

show that the hydrogen uptake increases with oxidation duration but with a decreasing rate at longer duration.

In addition, micro-analysis using EPMA, and µ-LIBS were carried out to map oxygen and hydrogen on a sample that underwent a ~400s long oxidation at 1200°C. The analysis revealed that hydrogen is mostly concentrated in the prior β-phase of the cladding. These analyses can also help identify any relationship between oxygen and hydrogen distribution in the material and investigate pseudo ternary $M5_{\mathbf{Framatome}}$-O-H phase diagram.

Influences of gap size, opening size and oxide layer effects on secondary hydriding are currently under investigation. Analytical segmented semi-integral tests are also planned. Simulations of these tests are underway with the SHOWBIZ code developed at IRSN (a new version of the code DIFFOX developed earlier at IRSN [18]).

AKNOWLEDGEMENT

The µ-LIBS measurements were performed at LASALYS (1 Avenue du Champ de mars, 45074 Orléans Cedex 2, France). The authors are grateful to the GGP – CC project for supporting this work. Additionally, the authors would like to thank Mrs. Gaelle VILLEVIEILLE for her contribution in preparing and performing the EPMA analysis.

References

[1] H.M. Chung, T.F. Kassner, Embrittlement criteria for Zircaloy fuel cladding applicable to accident situations in light-water reactors. Summary report, Argonne National Lab., IL (USA), 1980. https://www.osti.gov/biblio/5496633-embrittlement-criteria-zircaloy-fuel-cladding-applicable-accident-situations-light-water-reactors-summary-report (accessed July 18, 2022).

[2] H. Uetsuka, T. Furuta, S. Kawasaki, Zircaloy-4 Cladding Embrittlement due to Inner Surface Oxidation under Simulated Loss-of-Coolant Condition, J. Nucl. Sci. Technol. 18 (1981) 705–717. https://doi.org/10.1080/18811248.1981.9733309.

[3] H. Uetsuka, T. Furuta, S. Kawasaki, Fracture-bearing capability of zircaloy cladding on thermal-shock during the reflood stage of a loss-of-coolant accident in LWRs, Japan, 1983.

[4] F. Nagase, T. Fuketa, Effect of pre-hydriding on thermal shock resistance of zircaloy-4 cladding under simulated loss-of-coolant accident conditions, J. Nucl. Sci. Technol. Tokyo. 41 (2004) 723–730.

[5] F. Nagase, T. Chuto, T. Fuketa, Behavior of High Burn-up Fuel Cladding under LOCA Conditions, J. Nucl. Sci. Technol. 46 (2009) 763–769. https://doi.org/10.1080/18811248.2007.9711583.

[6] M. Billone, Y. Yan, T. Burtseva, R. Daum, Cladding embrittlement during postulated loss-of-coolant accidents., Argonne National Lab. (ANL), Argonne, IL (United States), 2008. https://doi.org/10.2172/946677.

[7] M. Flanagan, P. Askeijung, A. Puranen, Post-Test Examination Results from Integral, High-Burnup, Fueled LOCA Tests at Studsvik Nuclear Labo, U.S. Nuclear Regulatory Commission's, 2013. https://www.nrc.gov/reading-rm/doc-collections/nuregs/staff/sr2160/index.html (accessed March 20, 2023).

[8] J. Stuckert, M. Große, C. Rössger, M. Klimenkov, M. Steinbrück, M. Walter, QUENCH-LOCA program at KIT on secondary hydriding and results of the commissioning bundle test QUENCH-L0, Nucl. Eng. Des. 255 (2013) 185–201. https://doi.org/10.1016/j.nucengdes.2012.10.024.

[9] J. Stuckert, M. Grosse, M. Steinbrueck, M. Walter, A. Wensauer, Results of the QUENCH-LOCA experimental program at KIT, J. Nucl. Mater. 534 (2020) 152143. https://doi.org/10.1016/j.jnucmat.2020.152143.

[10] R. Thieurmel, J. Besson, E. Pouillier, A. Parrot, A. Ambard, A.-F. Gourgues-Lorenzon, Contribution to the understanding of brittle fracture conditions of zirconium alloy fuel cladding tubes during LOCA transient, J. Nucl. Mater. 527 (2019) 151815. https://doi.org/10.1016/j.jnucmat.2019.151815.

[11] J.-C. Brachet, D. Hamon, M. Le Saux, V. Vandenberghe, C. Toffolon-Masclet, E. Rouesne, S. Urvoy, J.-L. Béchade, C. Raepsaet, J.-L. Lacour, G. Bayon, F. Ott, "Study of secondary hydriding at high temperature in zirconium based nuclear fuel cladding tubes by coupling information from neutron radiography/tomography, electron probe micro analysis, micro elastic recoil detection analysis and laser induced breakdown spectroscopy microprobe, J. Nucl. Mater. 488 (2017) 267–286. https://doi.org/10.1016/j.jnucmat.2017.03.009.

[12] S. Leistikow, G. Schanz, Oxidation kinetics and related phenomena of zircaloy-4 fuel cladding exposed to high temperature steam and hydrogen-steam mixtures under PWR accident conditions, Nucl. Eng. Des. 103 (1987) 65–84. https://doi.org/10.1016/0029-5493(87)90286-X.

[13] L. Legras, E. Torres, M.C. Baietto, J. Desquine, A. Cabrera-Salcédo, M.B. Yriex, MLLS fitting on plasmon pic for mapping hydrides in a Zr alloy with a complex αZr+βZr acicular microstructure obtained by water quenching, in: Eur. Microsc. Congr. 2016 Proc., John Wiley & Sons, Ltd, 2016: pp. 1024–1025. https://doi.org/10.1002/9783527808465.EMC2016.5904.

[14] A. Hermann, H. Wiese, R. Bûhner, M. Steinemann, G. Bart, Hydrogen Distribution Between Fuel Cladding Metal and Overlaying Corrosion Layers, in: Park City, Utah, 2000.

[15] J.C. Brachet, D. Hamon, M.L. Saux, V. Vandenberghe, C.C. Toffolon-Masclet, E. Rouesne, S. Urvoy, J.L. Béchade, C.C. Raepsaet, J.L. Lacour, G. Bayon, F. Ott, Study of secondary hydriding at high temperature in zirconium based nuclear fuel cladding tubes by coupling information from neutron radiography/tomography, electron probe micro analysis, micro elastic recoil detection analysis and laser induced breakdown spectroscopy microprobe, J. Nucl. Mater. 488 (2017) 267. https://doi.org/10.1016/j.jnucmat.2017.03.009.

[16] R.E. Pawel, J.V. Cathcart, J.J. Campbell, S.H. Jury, Zirconium Metal-Water Oxidation Kinetics V. Oxidation of Zircaloy in High Pressure Steam, n.d.

[17] J. Desquines, C. Duriez, S. Guilbert, T. Taurines, High temperature oxidation and room temperature axial strength of pre-oxidized zircaloy-4 cladding after a simulated LOCA, J. Nucl. Mater. 543 (2021) 152559. https://doi.org/10.1016/j.jnucmat.2020.152559.

[18] C. Duriez, S. Guilbert, S. A., G. C., L. Belovsky, J. Desquines, Characterization of Oxygen Distribution in LOCA Situations, in: 2010. https://doi.org/10.1520/JAI103156.